(NASA-CR-173276) INVESTIGATION TO OPTIMIZE
THE PASSIVE SHOCK WAVE-BOUNDARY LAYER
CONTROL FOR SUPERCRITICAL AIRFOIL DRAG
REDUCTION Semiannual Report, 16 Mar. - 14
Sep. 1983 (Rensselaer Polytechnic Inst.,

N84-16135

Unclas
G3/02   15288

INVESTIGATION TO OPTIMIZE THE PASSIVE
SHOCK WAVE-BOUNDARY LAYER CONTROL FOR
SUPERCRITICAL AIRFOIL DRAG REDUCTION

BY

H.T. Nagamatsu, R. Ficarra, R. Orozco

Semi-Annual Report

for the period
March 16, 1983 to September 14, 1983

NASA Grant No. NAG-1-330

NASA Langley Research Center

Department of Mechanical Engineering,
Aeronautical Engineering & Mechanics
Rensselaer Polytechnic Institute
Troy, NY 12181

December 8, 1983

LIST OF SYMBOLS

A   —   cross-sectional area

A^* —   throat area

C   —   airfoil chord

C_d —   airfoil section drag coefficient

C_d' —   airfoil point drag coefficient

M   —   local Mach number

M_∞ —   freestream Mach number

P   —   static pressure

P_s —   static pressure in the wake

$P_{s\infty}$ —   free stream static pressure

P_0 —   impact pressure in the wake

P_{01} —   reference total pressure (ahead of shock)

P_{02} —   total pressure behind shock

x   —   distance from model leading edge

β —   shock wave angle

γ —   specific heat ratio

ABSTRACT

An investigation into the optimization of passive shock
wave/boundary layer control for supercritical airfoil drag reduction
was conducted in a 3 in. x 15.4 in. Transonic Blowdown Wind Tunnel.
A 14% thick NASA designed supercritical airfoil was tested with 0%,
1.42% and 2.8% porosities at Mach numbers of .70 to .83. The 1.42%
case incorporated a linear increase in porosity with the flow direction
while the 2.8% case was uniform porosity. The static pressure distri-
butions over the airfoil, the wake impact pressure data for determining
the profile drag, and the Schlieren photographs for porous surface
airfoils are presented and compared with the results for solid-surface
airfoils. While the results show that linear 1.42% porosity actually
led to a slight increase in drag it was found that the uniform 2.8%
porosity can lead to a drag reduction of 46% at M = .81.

After this portion of the testing was completed, a Mahogany
insert was designed and installed in the test section's top wall to
attain Mach numbers above .83 and to allow accurate prediction of the
Mach number before a test was conducted. Both of these goals were
achieved with the maximum tunnel Mach number exceeding .90.

Finally two steps were taken to improve testing efficiency.
First a new airfoil model was designed and constructed with a removable
porous section. This promises to save considerable time and effort
by eliminating the need to construct a new model every time a new porous
surface is desired. Second, a Commodore Model 64 microcomputer was
obtained to speed and simplify data storage and reduction.

INTRODUCTION

The increasing cost of fuel for military and transport aircraft has created an urgent need to increase aircraft performance through refinements in aerodynamics. The r:duction of wing drag, especially at transonic cruise speeds, is one way of achieving this goal.

In this transonic flight regime a dramatic increase in the drag takes place as the drag divergence Mach number is reached. Here the supersonic region on the surface of the airfoil is terminated by a normal shock wave. Soon after this shock wave appears in the flow, the drag will increase rapidly with increasing freestream Mach number leading to the "drag rise Mach number." One of the main objectives of designing a wing for transonic speeds is to attain as high a "drag rise Mach number" as possible. In principle supercritical airfoils are shaped to delay the drag rise associated with energy losses caused by shock waves and flow separation.

To control the drag increase due to the shock wave/boundary layer interaction for conventional airfoils and supercritical airfoils at transonic Mach numbers, a research program on the passive shock wave/boundary layer control for drag reduction was suggested by Mr. Dennis Bushnell and Dr. Richard Whitcomb at the NASA Langley Research Center. The concept of the passive drag reduction consists of having a porous surface with a cavity underneath at the shock wave location. The high pressure downstream of the shock wave will force some of the boundary layer flow into the cavity and out ahead of the shock wave. By this method, the boundary layer will thicken ahead of the shock wave and send compression waves into the supersonic region, thereby decreasing the Mach number for the normal shock wave. By this shock

wave/boundary layer interaction process, the increase of entropy across

the shock waves will be lower and the boundary layer flow separation

will be minimized. Both of these effects tend to decrease the drag

at transonic speeds and research is being conducted to study and optimize

this phenomenon.

PART 2

EXPERIMENTAL APPARATUS

2.1 Transonic Wind Tunnel

The 3 in x 15.4 in Transonic Wind Tunnel at Rensselaer Polytechnic Institute is a conventional blow-down wind tunnel with atmospheric air intake. Figure 1 is a scale drawing of the layout and Figure 2 is a photograph of the tunnel. Components of the tunnel are discussed below.

2.1.1 Entrance and Air Dryer

The tunnel entrance has two gates, both of which must be opened before operation is possible. The first is a venetian- blind-like set up, and the second is a large metal plate.

A large cross section silica gel bed dries the incoming air. Heating elements within the bed, along with an air circulating system, reactivate the gel bed when its moisture content is too high.

2.1.2 Settling Chamber

The settling chamber has a rectangular cross section 33.9 inches high, 20 inches wide and 48 inches long. Air flow is smoothed through a bellmouth inlet and a series of fine mesh screens and honeycomb. Flow imperfections are broken up and decay as they travel through the settling chamber to the contraction section. A total pressure probe is mounted within the settling chamber.

3

2.1.3 Contraction Section

The contraction section is constructed of multiple layers of thin aircraft plywood epoxyed together. Longitudinal ribs give the section further rigidity. The inside walls were carefully contoured, sanded and varnished to maintain a smooth and uniform flow. Recent modification led to a more uniform and higher inlet Mach number as shown in Figure 3. The contraction inlet is 20 in. by 33.9 in. at its inlet and 3 in. wide by 15.4 in. high at its exit, as shown in Figure 1. This contraction by a factor of almost 15 is achieved in 24 inches to smooth the flow into the test section.

2.1.4 Test Section

The test section is constructed from both aluminum and 1.25 inch thick transparent plexiglass for the side walls. Both top and bottom walls are aluminum, the side walls are plexiglass with an aluminum plate covering for reinforcement. The first twenty inches has a constant rectangular cross section with a width of 3 in. and height of 15.4 in. From the twenty inch point to the test section exit, the top and bottom walls diverge by 0.7 inches each while the plexiglass walls each diverge 0.15 inches, as shown in Figure 4. This tapering allows for the experimentally measured boundary layer growth [6]. In addition, the first twenty inches of the tunnel top wall is of variable porosity [7] but remained closed during this experiment. A 4.25 in. radius semicircle was cut from the aluminum test section walls to permit Schlieren photographs to be taken of the flow over the

airfoil model. The airfoil model is mounted on the test section bottom wall, about 6 inches from the section inlet, as shown in Figures 5, 6. Adjustable wedges located near the test section exit change the ratio of test area to the throat area, A/A^*, to control the Mach number in the test section.

A thin slot which spans the test section bottom wall immediately in front of the airfoil model can be used to remove the tunnel boundary layer so a new boundary layer starts at the airfoil leading edge. The slot is connected to a two-inch diameter piping to the vacuum system, cf. Figure 6, and a valve in the piping is opened at the start of each test run.

2.1.5 Top Wall Insert

The design and construction of a Mahogany top wall insert was prompted by the inability of the tunnel to reach Mach numbers above .83 and by an apparent lack of correlation between the Mach number attained and the number of turns on the above mentioned adjustment-plate screw.

The later problem was especially serious since it made the process of determining the freestream Mach number before any formal run (data collection) a trial-and-error procedure. Often several runs were made before the desired Mach number was reached. The inconvenience and restriction on the research process was undesirable.

The main cause of the problem is the sensitivity of the local Mach number to slight variations in the local area ratio (A/A*) in the transonic region. Contributing to this problem were blockage effects from the model and boundary layer build-up on the tunnel walls. Both of these effects were taken into account in the contouring of the insert, as shown in Figure 26, t_sts were conducted after installation and the results were promising. Mach numbers in excess of .90 were achieved and the relation between the Mach number and the number of turns of the adjustment plate screw became highly predictable (cf. Figure 27).

2.1.6 Diffuser Section

Two 50 inch long diverging sections make up the diffuser. From a rectangular inlet of 3.3 in. by 16.8 in., the diffuser takes the flow into a 15.25 inch square cross section at the exit. Finally an octagonal section fits the square to a 16 in. diameter circular pipe just ahead of the quick-acting pneumatic valve which actually controls the tunnel flow.

2.1.7 Quick-Acting Pneumatic Valve

A 16-inch diameter quick-acting pneumatic valve is located between the 16 inch diameter vacuum pipe and the octogonal transition section, shown in Figure 1. A house air supply of 120 psi is connected to a six inch diameter pneumatic cylinder which is attached

to the valve for quick opening through a 110 volt solenoid valve.
This later valve is activated by turning a starting key mounted on a
control box near the manometer board, Figure 2. A variable timer
relay can be preset to keep the valve open for a specified time.
Tests have indicated that tunnel flow is established within 0.4
seconds of the valve's actuation. [1,3]

2.2 14 Percent Thick Supercritical Airfoil

An aluminum 14%-thick NASA supercritical airfoil [12] was
used throughout these experiments and is shown in Figures 5-7. The
model is based on 200 points for the upper surface contour which were
programed into a computerized milling machine. It has a four-inch
chord and a three-inch span.

2.2.1 Pressure Taps

Sixteen static pressure taps are located along the
centerline of the model top surface at x/c positions of 0, .027, .078,
.156, .235, .313, .399, .469, .563, .645, .711, .801, .844, .906,
.945, and .985. A tap at .031 is on the underside of the airfoil and
an off-centerline tap at .711 measures the cavity pressure.

2.2.2 Porosity

The porous region extends from 56% to 83% of the chord.
Holes 0.025 inches in diameter are evenly spaced in 18 rows of 38
holes each. Based on hole area divided by total airfoil area, the

porosity with all holes open is 2.8%. The holes can be plugged and cleared to permit any percentage opening less than 2.8% or any variation of porosity distribution. In this experiment, a porosity which increased linearly in the flow direction was tested and compared to the full open 2.8% uniform porosity and the fully closed 0% porosity. The linear porosity started at the 56% chord with all holes closed and went to the 83% chord with all holes in the row opened. The resulting porosity was 1.42% with linear variation of porosity.

2.2.3 Cavity

A cavity located beneath the porous surface is 3/4 inch deep and can be partially filled to simulate different cavity depths. Based on Bahi's results [1], a 1/4 inch deep cavity was selected and kept constant throughout this experiment. The drag reduction was greater for a 1/4 inch cavity than for a deeper cavity.

2.2.4   Supercritical Airfoil with Removable Porous

The enormous amount of time and effort required to machine a new airfoil model and to insert pressure taps prompted the design of a model with a removable porous section. This eliminates the need to construct entire models for each different porous surface. Instead many easily made removable sections can be used with a single model. Figures 28 and 29 reveal the details of the design.

2.3 Instrumentation

2.3.1 Pressure Taps and Manometer Board

Flush-mounted static pressure taps are located at various points along the transonic wind tunnel's side and bottom walls. An impact pressure probe located in the settling chamber gives the total pressure. Twenty mercury-filled U-tube manometers are connected to these taps by plastic tubing, as shown in Figures 2 and 5. An electrically timed solenoid valve system is used to capture the manometer readings and maintain them while the data is recorded.

2.3.2 Electrical Timing System

By turning a key on the control box mounted near the manometer board, the quick-acting pneumatic valve is activated. After a specified run time a delay timer relay closes the solenoid valves on the manometers while simultaneously activating the camera shutter on the Schlieren optical system. The flow-controlling valve then automatically closes.

2.3.3 Schlieren Optical System

A conventional single-pass Schlieren optical system was used to observe flow characteristics over the test model. A zirconium light source sent a focused beam to two flat 9.5 inch diameter mirrors and two parabolic 7.5 inch diameter mirrors, both with focal lengths of five feet, cf. Figure 8. An adjustable knife edge mounted on the camera stand was positioned at the last mirror's focal point. Either

a film plate holder or a smoked glass plate could be placed in the

camera for taking pictures or watching the flow over the airfoil,

respectively. Stress concentrations in the plexiglass apparently

created spots near the leading and trailing edges of the airfoil

model, and an oval scratch mark high on the semicircle were

characteristic of each Schlieren photograph.

2.3.4 Wake Survey Rake

The airfoil model wake impact pressures were measured using

a stainless steel rake mounted 1.75 inches downstream of the trailing

edge centerline. The rake height is 2.1 inches and has ten separate

probes spaced closely together near the tunnel bottom wall and spread

out as the vertical height increases. Each probe had an inner

diameter of .025 inches and an outer diameter of .035 inches. These

probes can be connected to the U-tube manometers.

2.3.5 Microcomputer Installation

A Commadore model 64 microcomputer was installed adjacent

to the wind tunnel to speed and simplify data reduction and storage.

Programs have been written to obtain profile drag coefficients

and Mach and Pressure distributions directly from manometer readings.

The human error factor has been greatly reduced and it is now

possible to reduce data for evaluation within ten minutes of running.

A program is being developed to plot the experimental results

by the computer.

2.3.6 <u>Vacuum Pumps</u>

Six 5-hp vacuum pumps operate continuously to evacuate a large 2000 cubic foot vacuum tank to a minimum pressure of about one inch of mercury. The pressure difference across the pneumatic valve establishes the flow in the tunnel when the valve is opened.

PART 3

THEORY

Data reduction in this experiment was based on the basic compressible flow relation under the assumptions of steady, perfect isentropic gas flow [14].

3.1 Mach Number

Local Mach numbers in the transonic tunnel were calculated by using local static pressures, P, and total pressure from the settling chamber, P_{01}, assumed everywhere to be constant. The static pressure ratio is given by

$$\frac{P_{01}}{P} = \left(1 + \frac{\gamma-1}{2} M^2\right)^{\frac{\gamma}{\gamma-1}} , \qquad (1)$$

and rearranging this equation to find the Mach number by

$$M = \left\{ \left[\left(\frac{P_{01}}{P}\right)^{\frac{\gamma-1}{\gamma}} - 1 \right] \frac{2}{\gamma-1} \right\}^{1/2} \qquad (2)$$

where γ was assumed to be constant, 1.40.

3.2 Drag Coefficient

The drag coefficient can be obtained by calculating the point drag coefficient and then integrating across the wake. The point drag coefficient is derived from an evaluation of the momentum

13

loss in the airfoil wake. Several schemes for the evaluation of point drag coefficient were studied, References 8-10, but the following expression was used from Reference 11:

$$C_d' = 2\left[\frac{P_0}{P_{01}}\right]^{\frac{\gamma-1}{\gamma}} \left[\frac{P_s/P_{01}}{P_{s\infty}/P_{01}}\right]^{\frac{1}{\gamma}} \left\{\frac{1-\left[\frac{P_s/P_{01}}{P_0/P_{01}}\right]^{\frac{\gamma-1}{\gamma}}}{1-[P_{s\infty}/P_{01}]^{\frac{\gamma-1}{\gamma}}}\right\}^{\frac{1}{2}} \left\{1-\left\{\frac{1-\left[\frac{P_{s\infty}/P_{01}}{P_0/P_{01}}\right]^{\frac{\gamma-1}{\gamma}}}{1-[P_{s\infty}/P_{01}]^{\frac{\gamma-1}{\gamma}}}\right\}^{\frac{1}{2}}\right\} \quad (3)$$

The drag coefficient for the airfoil is calculated by integrating across the wake,

$$C_d = \frac{1}{c} \int_{wake} C_d' \, dy \quad (4)$$

According to Equation (3) for the point drag coefficient, it can be seen that if the impact pressure ratio $\frac{P_0}{P_{01}} = 1.0$ the expression is equal to zero. Further if $\frac{P_0}{P_{01}} > 1.0$ the expression gives a negative point drag coefficient. Theoretically the negative should never occur because no local pressure will exceed the total stagnation pressure, P_{01}. Experimentally, however, this has occured, giving rise to examination of the equation and the accuracy of measuring the impact pressure in the wake region.

PART 4

DISCUSSION OF RESULTS

The way to achieve passive drag control, as discussed previously, is to place a porous surface in the chordwise region of the normal shock wave. Part of the boundary layer flow downstream of the shock will move upstream through the porous surface and the cavity, as shown in Figure 9. Two important results of this recirculated flow are to reduce boundary layer separation and shock wave strength. By removing the decelerated flow behind the shock, the thinner boundary layer tends to remain attached. And by sending the decelerated flow ahead of the shock, compression waves gradually build into a shock wave of reduced strength. The combination of these resulting phenomena helps reduce wave drag on airfoils operating at transonic speeds, which was the purpose of this investigation.

4.1 Schlieren Photographs

Flow characteristics over the 14%-thick supercritical airfoil were recorded with Schlieren photography. The Schlieren photographs of the flow for three porosities are presented in Figures 10-12 for 0% porosity, 2.8% uniform porosity, and 1.42% linear porosity and different flow Mach numbers.

Figures 10a and 10b show flow over the airfoil model when all the porous plate holes were plugged, i.e. 0% porosity. Figure 10a, at a freestream Mach number of 0.808, shows a thicker shock wave than Figures 11, with a shock which is nearly normal to the airfoil

15

surface and curving upward. Figures 10b, at a freestream Mach number of 0.826, shows the same characteristics as Figure 10a, with compression waves coalescing to form the shock wave.

Figures 11 a-e show flow over the airfoil with 2.8% uniform porosity and different flow Mach numbers. Figure 11a is a Schlieren photograph of flow at a freestream Mach number of 0.736. No flow disturbances are seen, which is expected since the critical Mach number is about 0.75. In Figure 11b the freestream Mach number has been increased to 0.809 and a small λ-shock wave appears with a few compression waves forming upstream. At a Mach number 0.82, Figure 11c, a larger λ-shock wave dominates the picture with a strong front leg and a series of compression waves forming into a weaker rear leg. A thin aftershock appears just behind the rear leg, but does not seem to meet the airfoil surface. In Figure 11d the freestream Mach number is 0.827 and a large λ-shock has characteristics much like Figure 11c except this shock wave has longer legs and is spread out more. The aftershock has merged with the rear leg or disappeared. For a freestream Mach number of 0.832, Figure 11e shows the highest Mach number the tunnel was operated at. Here the λ-shock wave spans the entire length of porous plate and seems to extend downstream some. At least ten compression waves can be clearly seen to form into the main shock. Figure 12 is a Schlieren photograph of flow at a freestream Mach number of 0.815 over the airfoil with 2.8% uniform porosity which clearly shows some boundary layer/shock wave interaction on the rear leg of the λ-shock wave.

Figures 13a and 13b show flow over the airfoil with a 1.42%
linear porosity. Figure 13a for a freestream Mach number of 0.80
shows a backward S-shaped shock with compression waves. The same
shock wave characteristics at a Mach number of 0.82 are evident in
Figure 13b.

4.2 Shock Wave Shape and Location

With 2.8% uniform porosity, as the freestream Mach number
increases, the λ-shock wave can be seen to become greater with the
λ-shock waves becoming longer and more spread apart to span the porous
surface. Only two Schlieren photographs are presented for 0% and
1.42% linear porosity because the shock shapes are very nearly
constant with Mach number. The 0% porosity shapes were slightly
curved but normal at the model surface. These shock waves were
thicker than both 2.8% uniform and 1.42% linear porosity cases, and
extended further upward in height. Like the 2.8% uniform case, the
1.42% linear porosity shock waves had many compression waves leading
into the main shock. The backward S-shape remained constant with Mach
number.

Tracings of shock wave shapes were taken from the Schlieren
photographs for all porosities at various Mach numbers. These are
presented in Figure 14. Shock waves for all porosities moved rearward
with increasing Mach number. A graph of the shock wave x/c position
as a function of the freestream Mach number is presented in Figure 15.

When observing this graph keep in mind the porous plate extends from
56% to 83% chord. The 2.8% uniform porosity has two shock waves, the
front oblique shock wave remaining nearly constant near the front edge
of the porous surface. The rear shock wave moves rearward with
increasing Mach numbers. The 0% porosity shows a rearward movement
with increasing Mach number, but with a 'slope' of less than 1/2 of
the 2.8% uniform porosity case. Thus, the porosity allows the shock
wave to move rearward more quickly, keeping the boundary layer
separation minimized. The 1.42% linear porosity has nearly the same
shock wave location change in x/c position with Mach number as the
2.8% uniform porosity configuration. Hence, both porosities have a
similar effect on the shock wave location.

4.3 Mach Distribution

Local airfoil model Mach number distributions for all
porosities at a freestream Mach number of 0.804 are presented in
Figure 16a and at a freestream Mach number of 0.826 in Figure 16b. In
Figure 16a the Mach number distributions for all porosities are the
same up to 50% chord. The 0% porosity shows a sharp change in the
Mach number indicating the presence of a strong shock wave. For the
2.8% uniform porosity the changes in the Mach number distribution are
more gradual indicating a weak shock wave and a weaker pressure
gradient. The Mach number distribution for 1.42% linear porosity is
between the other two cases. The sonic line, M=1.0, can be seen to
start at 10% chord in all cases. A 'hump' in the Mach number

distribution curves at the 83% chord location can be explained by the change in porosity at that point.

Figures 17a and 17b show Mach number distributions for 0% and 2.8% uniform porosities at various freestream Mach numbers, respectively. These curves show how the local Mach number changes with increasing Mach number. Sharp decreases in the Mach number indicate some very strong shock waves in Figure 17a. Figure 17b shows more gradual transitions from supersonic to subsonic Mach numbers.

4.4 Drag Distribution

Figures 18a and 18b plot local point drag coefficient vs. vertical rake height for various porosities at freestream Mach numbers of 0.804 and 0.826 respectively. The area under each curve represents the integrated drag coefficient for that curve. All graphs drop quickly at first: a factor of ten by 1/2 inch into the wake. They usually continue past 2.0 inches due to shock wave influence.

The drag coefficients for various porosities are presented in Figures 19 a-d as a function of the freestream Mach number. In Figure 19d the drag coefficients for the three porosity configurations are plotted together in order to compare the results. For all porosities the drag coefficient increases with the freestream Mach number. With the 2.8% porosity configuration, the rapid increase in the drag occurs at a higher Mach number than for either 0% or 1.42% porosities. However, the drag coefficient for the 2.8% porosity case is slightly higher before its rapid increase than the other

configurations for Mach numbers less than 0.78. At high Mach numbers
the shock wave/boundary layer concept produces oblique shock waves and
lowers the drag coefficient by decreasing the entropy increase and the
boundary layer thickness compared to the solid suface with a normal
shock wave. At lower Mach numbers without the shock waves the holes
act more like a roughness with flow through the cavity resulting in
higher drag than the smooth 0% porosity airfoil.

The variation of the drag coefficient for the 1.42% linear
porosity configuration with freestream Mach number is consistently
higher than for the solid surface with 0% porosity. Apparently this
smaller percentage of porosity with linear variation in the porosity
distribution from the leading edge of the cavity prevents the shock
wave/boundary layer concept from being effective and merely disturbs
the flow. Therefore, the proper percentage and distribution of
porosity are important for decreasing the supercritical airfoil drag
at transonic Mach numbers.

In Table 1 the drag coefficient and the percentage decrease
in the drag with the 2.8% porosity compared to the results for the
solid airfoil surface are presented for various freestream Mach
numbers. For freestream Mach numbers of 0.78 to 0.81 at which
commercial aircraft operate, a decrease in the airfoil top surface
drag coefficient up to 46% was obtained with the uniform 2.8% porosity
from the drag for the solid surface configuration.

4.5 Pressure Investigations

Static pressure ratios across the shock wave, P_2/P_1, are

presented as functions of freestream Mach number for 0% and 2.8% porosities in Figure 20. As predicted by theory, the pressure ratio increases with Mach number. The pressure ratio remains much closer to 1.0 for 2.8% porosity than for the 0% porosity, verifying that the pressure gradient behind the shock wave is weaker with porosity.

The stagnation pressure ratios across the shock wave, P_{02}/P_{01}, are presented as functions of freestream Mach number for 0% and 2.8% uniform porosity in Figure 21. A stagnation pressure ratio close to 1.0 is a measure of a weak shock wave and as the ratio decreases, the shock wave losses increase. Figure 21 shows that the ratio for 2.8% uniform porosity stays quite close to 1.0 with Mach number while for 0% porosity the ratio is lower and decreases with Mach number. Hence, the porosity decreases the shock losses by producing a λ-shock wave over the airfoil as shown in Figure 11.

The total stagnation pressure ratio decrease across a shock wave was taken into account when calculating the Mach distribution over the model after the shock wave, as seen in Figure 22 for a freestream Mach number of 0.826 and 0% porosity and shows a slight decrease in local Mach number.

As a demonstration of the calculation procedure, the method is outlined here. The shock wave was assumed to be a Mach line which obeys the expression $\sin \beta = \frac{1}{M}$. The shock wave angle β was measured from the Schlieren photograph to be 51 degrees, for a freestream Mach number of 0.826, and the Mach number calculated is 1.287. As a check, the Mach distribution shows a local Mach number of 1.285 which is good

agreement. Using this Mach number a total pressure ratio of $P_{02}/P_{01} =$ .9816 was used to correct for the total pressure loss and the local Mach number was recalculated, as shown in Figure 22.

The maximum local Mach numbers are presented in Figure 23 as functions of freestream Mach number for both 0% and 2.8% porosities. The figure shows that the critical Mach number where sonic flow is first attained on the airfoil surface is approximately 0.75. M_1 rises less rapidly for 2.8% porosity than for 0%, indicating a more uniform flow for 2.8% porosity, which minimizes the boundary layer separation.

A local flow Mach number survey along the length of the transonic wind tunnel was taken and is shown in Figure 24. At 90 inches downstream of the inlet bellmouth, the flow speed equaled the local sonic velocity and apparently was the effective tunnel throat. The test section extends from 72 inches to 108 inches downstream of the bellmouth. The adjustable wedges which change the freestream Mach number are located between 90 and 100 inches downstream. The local Mach number reaches its maximum value (M = 1.62) at 120 inches and decreases rapidly through the diffuser section.

Typical wake impact pressure ratios are presented as functions of vertical height in Figure 25 for 0% and 2.8% porosities. For the 2.8% porosity the pressure ratio increases rapidly from a value of about 0.64 at the tunnel floor to 0.96 just 1/4 inch from the floor and then increases slowly through the rest of the wake. For the 0% porosity case the pressure increases less rapidly from 0.64 to 0.96 in 1/2 inch and then follows the same trend as 2.8% porosity.

PART 5

SUMMARY

Passive shock wave/boundary layer control for 0%, 1.42%
linear and 2.8% uniform porosities was investigated using a 14% thick
supercritical airfoil in a transonic wind tunnel. Extensive
comparisons of the shock wave shape and location, Mach number, drag
distributions, and pressure studies were made for each porosity. The
following is a summary of the results:

- The shock wave shape for 0% porosity was nearly normal; for
  1.42% linear porosity it was S-shaped and for 2.8% uniform a
  λ-shock wave which grew in size with increasing Mach number
  was observed.

- For all porosities, the shock wave moved rearward with
  increasing Mach number. The Mach number distributions
  indicated a sharply changing Mach number for 0% porosity, but
  a gradual change for both 1.42% and 2.8% porosities.

- The sonic line on the airfoil was at 10% chord and the
  critical flow Mach number was about 0.75 for 0% porosity.

- The drag coefficient increases rapidly at high flow Mach
  numbers for all porosities. The drag coefficient for the 2.8%
  uniform porosity is lower than for 0% and 1.42% linear
  porosities at Mach numbers greater than 0.78, but higher at
  Mach numbers below 0.78. This effect is due to the porous
  surface and the cavity. 1.42% porosity surprisingly has a

23

higher drag coefficient than 0% porosity possibly due to the
unexpected flow interactions.

- Both static and stagnation pressure ratios were more favorable
  to keep shock wave losses down for the 2.8% uniform porosity
  case than for the 0% porosity case. The wake impact pressure
  ratio for 0% porosity indicated a wake region about twice as
  thick as for 2.8% uniform porosity.

PART 6

CONCLUSIONS

The concept of passive shock wave/boundary layer control for transonic drag reduction has already been proved. One of the objectives of this study was to show how well it worked for various porosities. The 1.42% linear porosity failed to improve the drag characteristics of the airfoil, and in fact made them worse than no porosity.

The concepts which were theorized to make passive shock wave/boundary layer control work were verified as shown by the lower stagnation pressure loss with the 2.8% uniform porosity. Additionally, for a freestream Mach number of 0.81, the profile drag coefficient for the airfoil top surface with uniform porosity showed a 46% decrease from the solid surface airfoil.

Schlieren photographs indicated the details of the shock waves including the compression waves and boundary layer interaction. The photographs of the flow over the airfoil for various configurations led to a better understanding of the effect of the porous surface with cavity.

PART 7

REFERENCES

1. Bahi, L., "Passive Shock Wave/Boundary Layer Control for Transonic Supercritical Airfoil Drag Reduction," Ph.D. Thesis, Department of Aeronautical Engineering, Rensselaer Polytechnic Institute, Troy, New York, May 1982.

2. Ross, J., "Passive Shock Wave/Boundary Layer Control for Drag Reduction on a Convex Transonic Airfoil," M.S. Thesis, Department of Aeronautical Engineering, Rensselaer Polytechnic Institute, Troy, New York, May 1982.

3. Bidlack, T., "Top Wall Blockage Effects on Passive Shock Wave Boundary Layer Control for a Supercritical Airfoil," M.S. Thesis, Department of Aeronautical Engineering, Rensselaer Polytechnic Institute, Troy, New York, August 1982.

4. Maestrello, L., "Initial Results of a Porous Plug Nozzle for Supersonic Jet Noise Suppression," NASA-TM 78802, November 1978.

5. "Perforated Wing Saves Fuel," Aviation Week and Space Technology, Volume 21, May 24, 1982, pages 60, 61.

6. Nagamatsu, H., Brower, W., Bahi, L. and Marble, S., "Investigation of Passive Shock Wave/Boundary Layer Control for Transonic Airfoil Drag Reduction," First Annual Report, NASA Grant No. NSG 1624, October 1980.

7. Marble, S., "Transonic Wind Tunnel Blockage Minimization Using a Variable Porosity Plate," M.Eng. Thesis, Department of Mechanical Engineering, Rensselaer Polytechnic Institute, Troy, New York, May 1981.

8. Baals, D. and Mourhess, M., "Numerical Evaluation of the Wake-Survey Equations for Subsonic Flow Including the Effect of Energy Addition," Advanced Restricted Report L5H27, Langley Field, Virgina, November, 1945.

9. Lock, C., Hilton, W., and Goldstein, S., "Determination of Profile Drag at High Speeds by a Pitot Traverse Method," Reports and Memoranda No. 1971, British A.R.C., September, 1940.

10. Silverstein, A. and Katzoff, S., "A Simplified Method for Determining Wing Profile Drag in Flight," Journal of Aeronautical Science, Volume 7, No. 7, May 1940.

11. Pankhurst, R.C., and D.W. Holder, <u>Wind Tunnel Technique</u>. Sir
    Isaac Pitman and Sons, Ltd., London, 1965.

12. Harris, C.D., "Aerodynamic Characteristics of a 14 Percent Thick
    NASA Supercritical Airfoil Designed for a Normal Force
    Coefficient of .7," NASA TMX-72712, 1975.

13. Thiede, P., "Supercritical Airfoil Flow Control by Slot Suction
    in the Shock Region," DEA AFFDR-TR-80-3088, April 1980.

14. Liepman, H.W. and A. Roshko, <u>Elements of Gasdynamics</u>, Wiley, 1957.

15. Orozco, R. "Foeosity Effects on Supercritical Airfoil Drag
    Reduction by Shock Wave/Boundary Layer Control," M.S. Thesis,
    Department of Aeronautical Engineering. Rensselaer Polytechnic
    Institute, Troy, NY, May 1983.

Freestream Mach Number	Drag Coefficient		Percentage Change $\dfrac{C_d(0) - C_d(2.8)}{C_d(0)}$
	0%	2.8%	
.76	.030	.039	−30
.77	.034	.040	−18
.78	.040	.041	−3
.79	.C48	.0425	11
.80	.060	.044	27
.805	.070	.045	36
.81	.085	.046	46

Table 1   Percentage Change in Drag Coefficient Using Shock Wave/Boundary Layer Control

19.54 ft
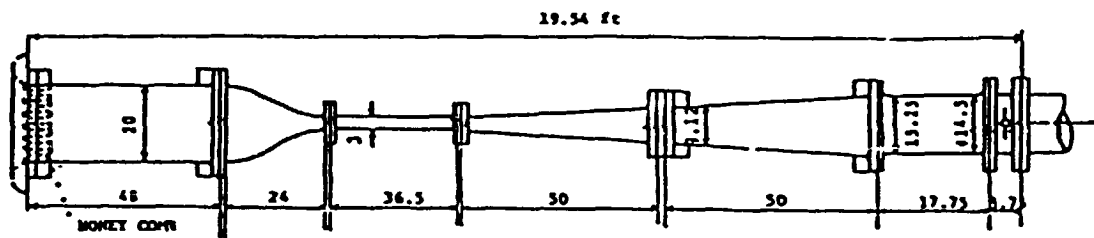
Top view
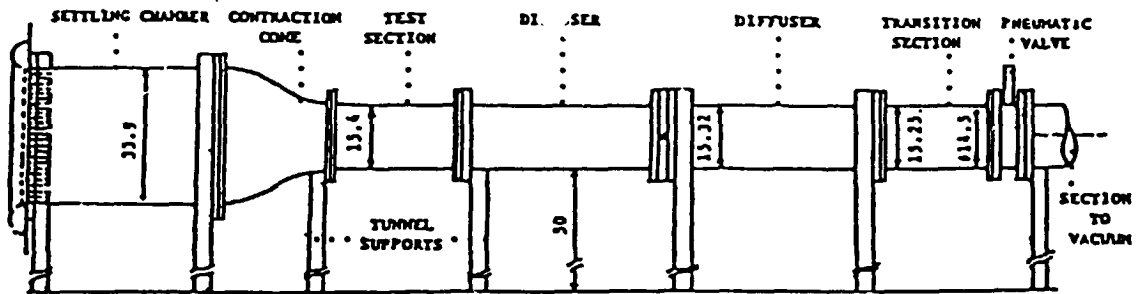
Side view

Fig.1 Scale drawing of 3x15.4 inch Transonic Wind Tunnel

Figure 2   Photograph of Transonic Wind Tunnel
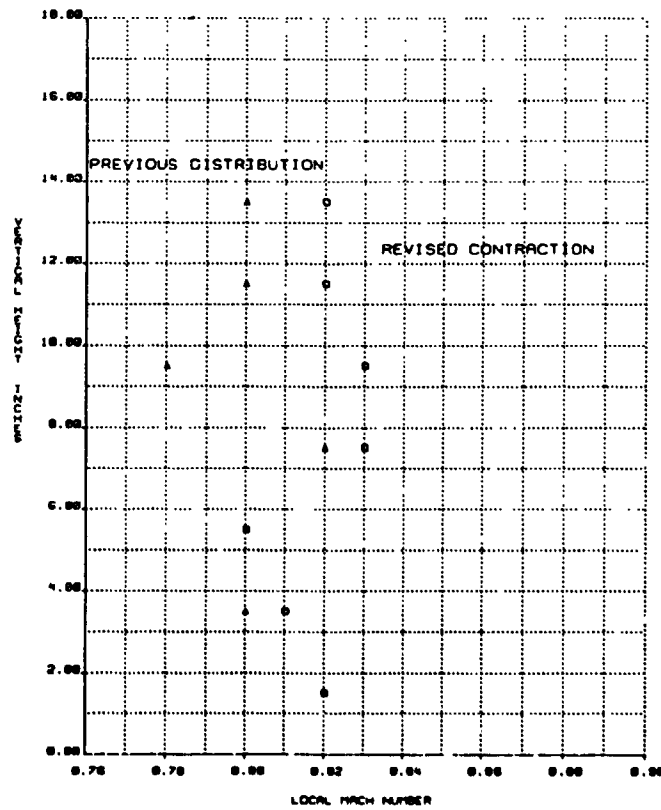
Figure 3   Mach Distribution for Test Section Entrance
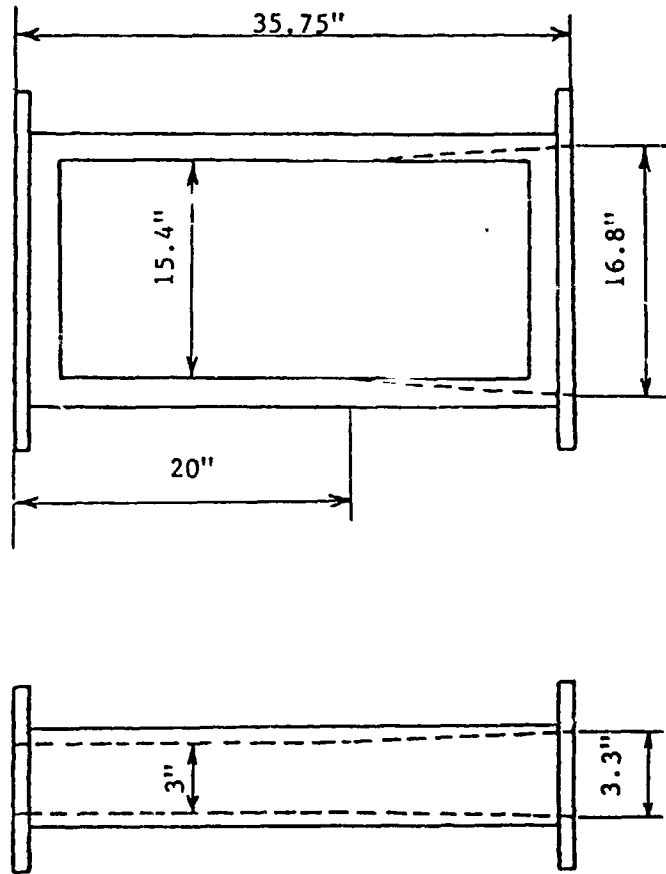
Figure 4   Test Section Modified to Accomodate Boundary
Layer Growth

Figure 5   Photograph of Test Section

Airfoil surface

Porous surface

Cavity

Boundary layer removal
system
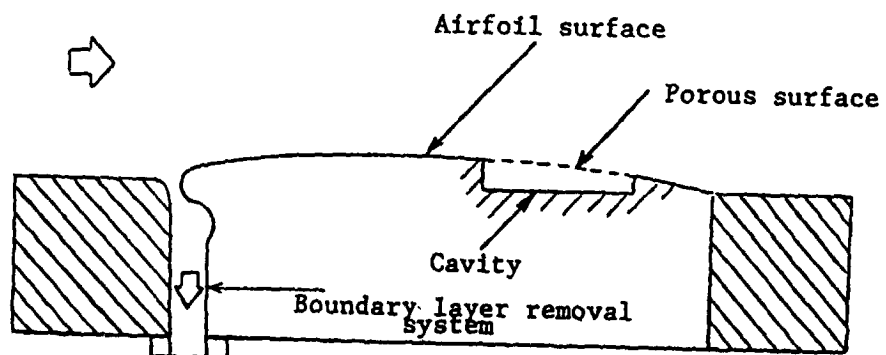
Figure 6   Schematic of Airfoil Model in Test Section

Figure 7   Photograph of Supercritical Airfoil Model
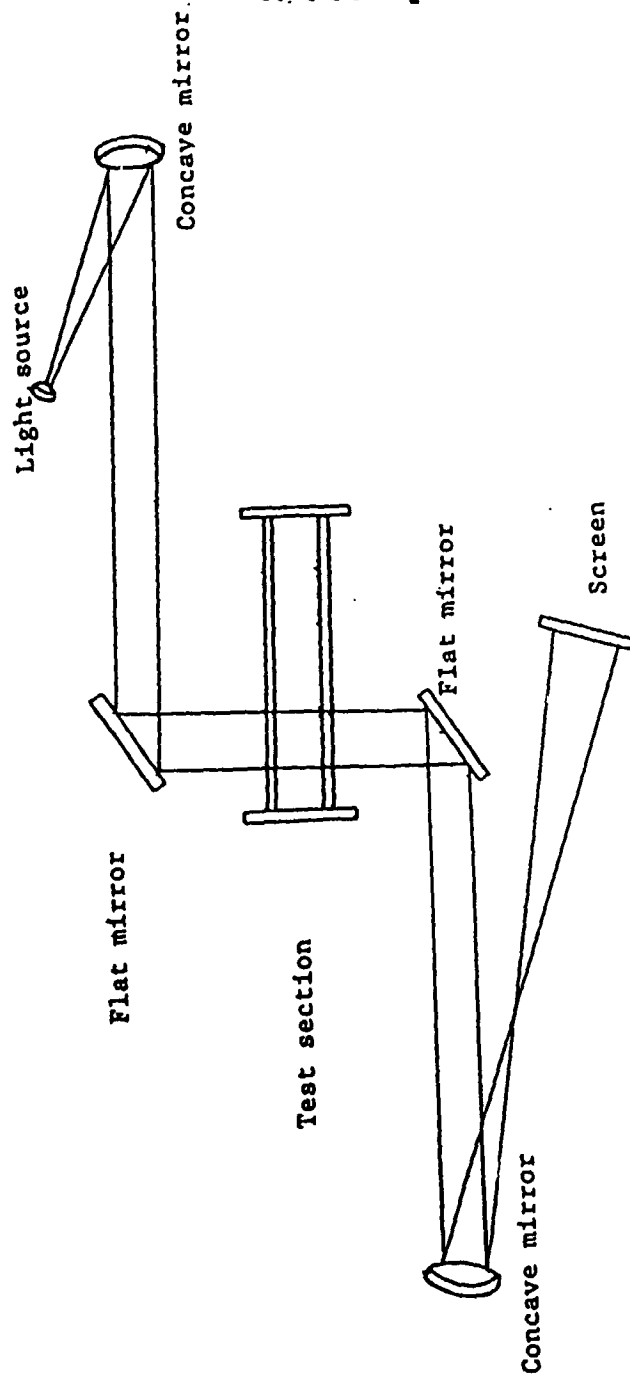
Fig. 8 Schematic of the Schlieren optical system

1. Supercritical airfoil
2. Porous surface
3. Cavity beneath porous surface
4. Free stream conditions
5. Embedded supersonic region
6. Sonic line
7. Terminating shock wave
8. Flow circulation through the porous surface
9. Wake survey rake
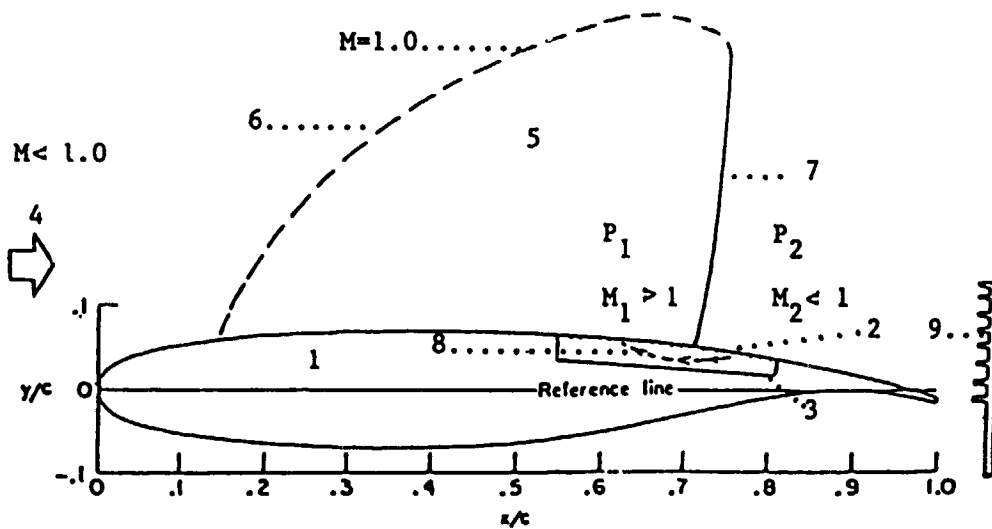
Fig. 9 Passive drag control for supercritical airfoil
at transonic Mach numbers

Figure 10a Schlieren Photograph of Airfoil with 0% Porosity
$M_\infty = 0.808$

Figure 10b Schlieren Photograph of Airfoil with 0% Porosity
$M_\infty = 0.826$

Figure 11a   Schlieren Photograph of Airfoil with 2.8% Uniform
Porosity, $M_\infty = 0.736$

Figure 11b   Schlieren Photograph of Airfoil with 2.8% Uniform
Porosity, $M_\infty = 0.809$

Figure 11c Schlieren Photograph of Airfoil with 2.8% Uniform
Porosity, $M_\infty = 0.82$

Figure 11d Schlieren Photograph of Airfoil with 2.8% Uniform
Porosity, $M_\infty = 0.827$
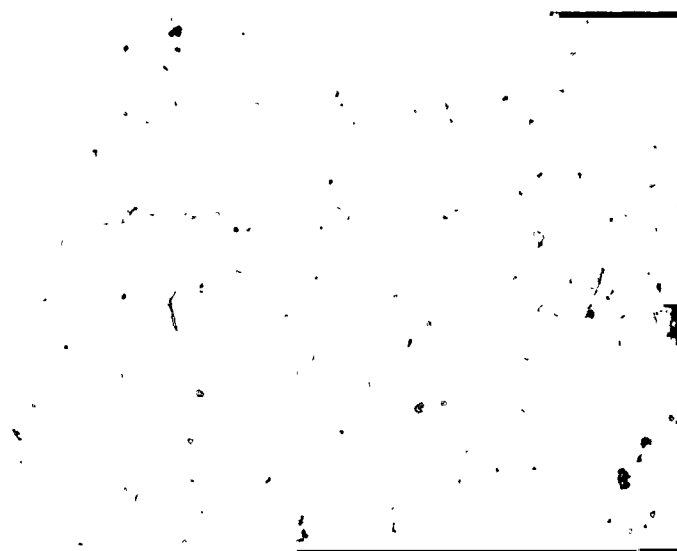
Figure 11e   Schlieren Photograph of Airfoil with 2.8% Uniform
Porosity, $M_\infty = 0.832$
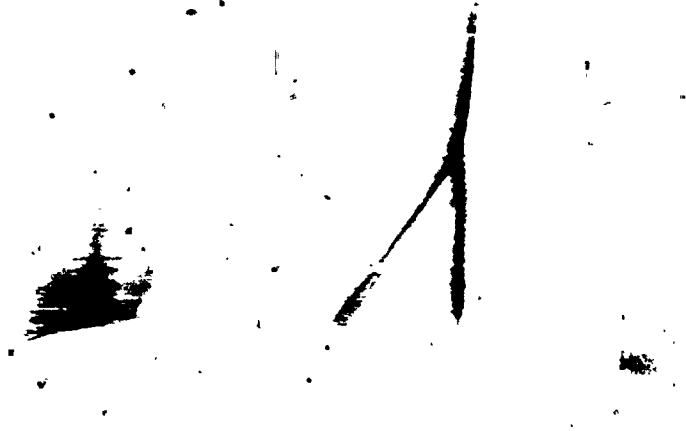
Figure 12 Schlieren Photograph showing Shock Wave/Boundary Layer
Interaction on Rear Leg of Shock, $M_\infty = 0.819$
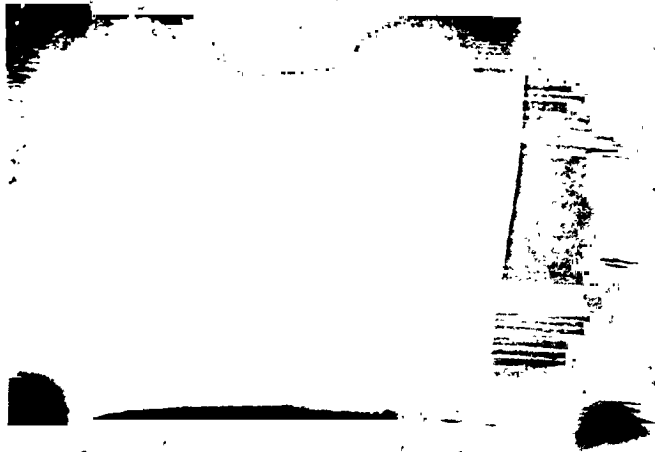
Figure 13a Schlieren Photograph of Airfoil with 1.42% Linear
Porosity, $M_\infty = 0.80$
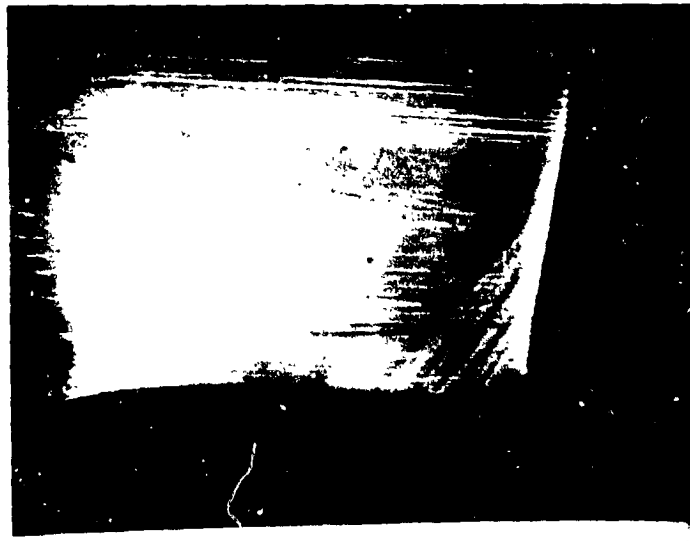
Figure 13b Schlieren Photograph of Airfoil with 1.42% Linear
Porosity, $M_\infty = 0.82$

2.8% Uniform Porosity

$M_\infty = .809$ $M_\infty = .82$ $M_\infty = .83$

0% Porosity

$M_\infty = .808$ $M_\infty = .826$ $M_\infty = .83$

1.42% Linear Porosity

$M_\infty = .80$ $M_\infty = .82$
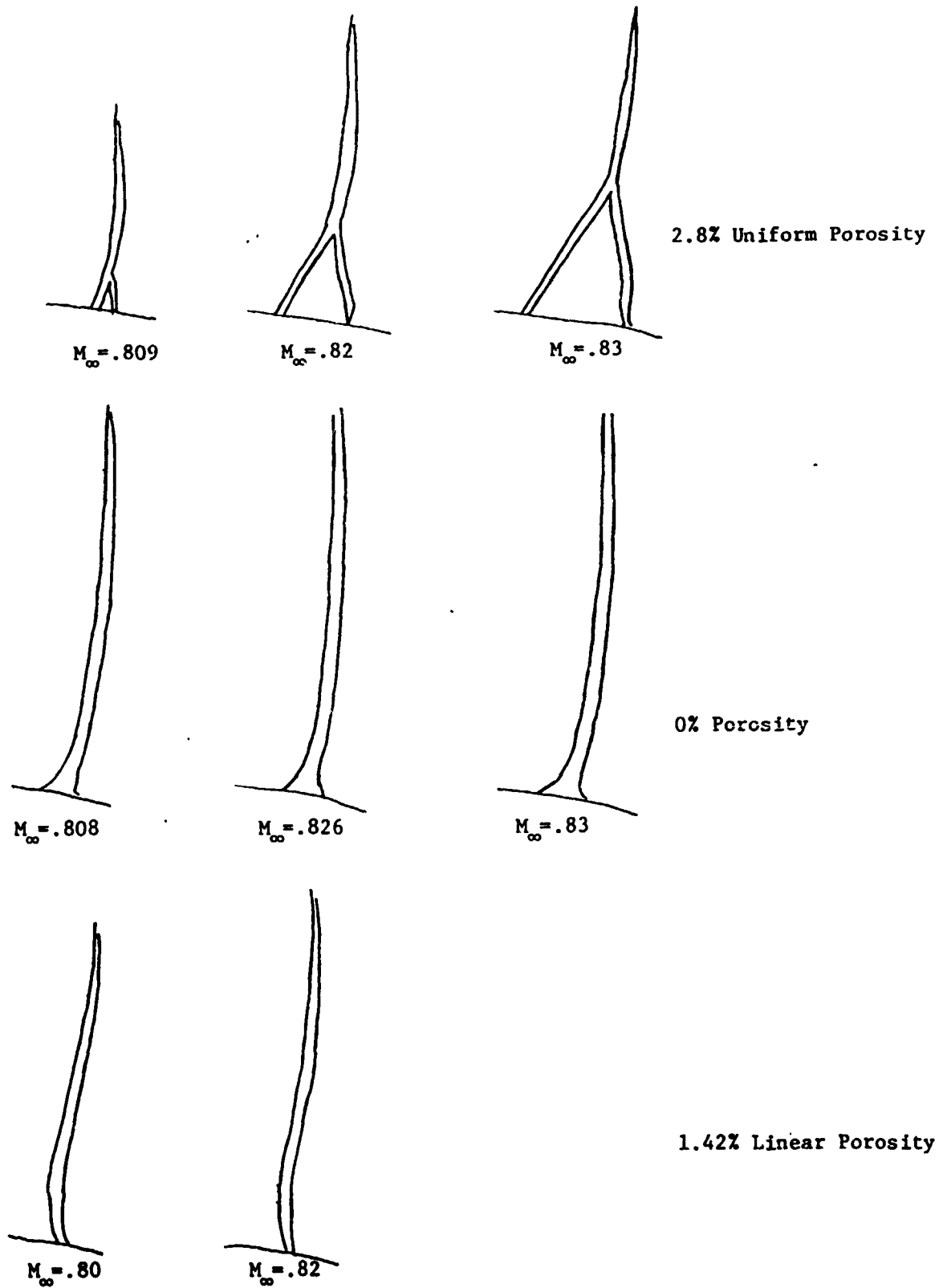
Figure 14   Tracings of Shock Wave Shapes for 0%, 2.8% and 1.42%
Porosities at Various Freestream Mach Numbers

Figure 15   Shock Location vs. Freestream Mach Number on a 14%-Thick
Supercritical Airfoil for 0%, 1.42% and 2.8% Porosities.

Figure 16a   Mach Number Distribution over Airfoil with 0%, 1.42%
and 2.8% Porosities, M_∞=0.804
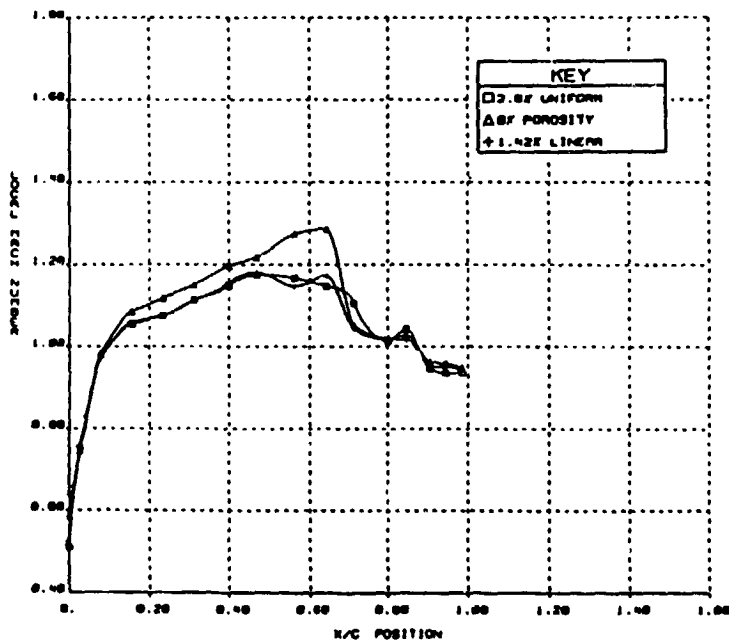
Figure 16b   Mach Number Distribution over Airfoil with 0%, 1.42%
and 2.8% Porosities, M_∞=0.826

Figure 17a   Mach Number Distribution over Airfoil with 0% Porosity at Various Freestream Mach Numbers
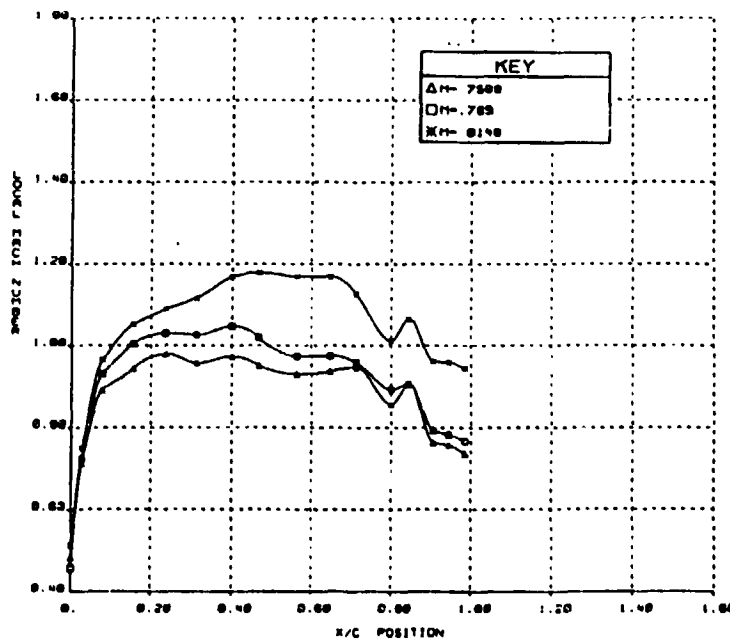
Figure 17b   Mach Number Distribution over Airfoil with 2.8% Uniform Porosity at Various Freestream Mach Numbers

Figure 18a   Point Drag Coefficient Distribution for 0%, 1.42%
and 2.8% Porosities, $M_\infty=0.804$
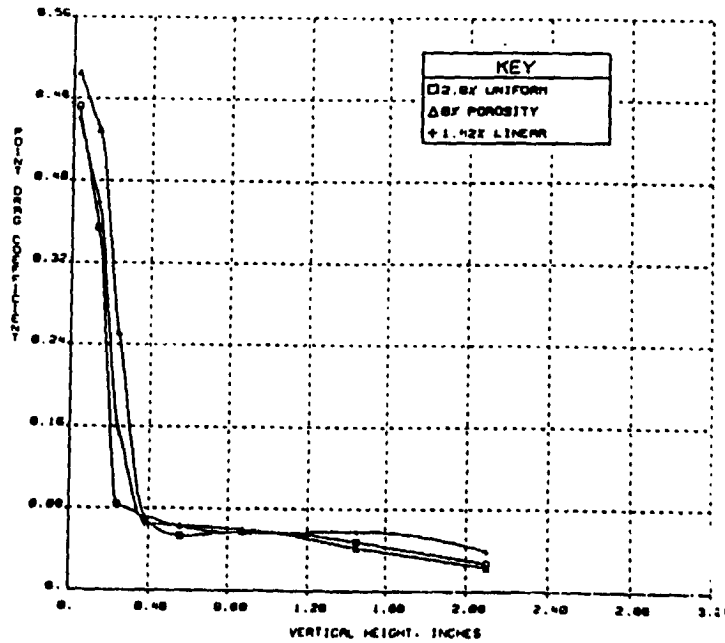
Figure 18b   Point Drag Coefficient Distribution for 0%, 1.42%
and 2.8% Porosities, $M_\infty=0.826$

Figure 19a   Drag Coefficient vs. Freestream Mach Number,
0% Porosity

Figure 19b   Drag Coefficient vs. Freestream Mach Number,
2.8% Porosity
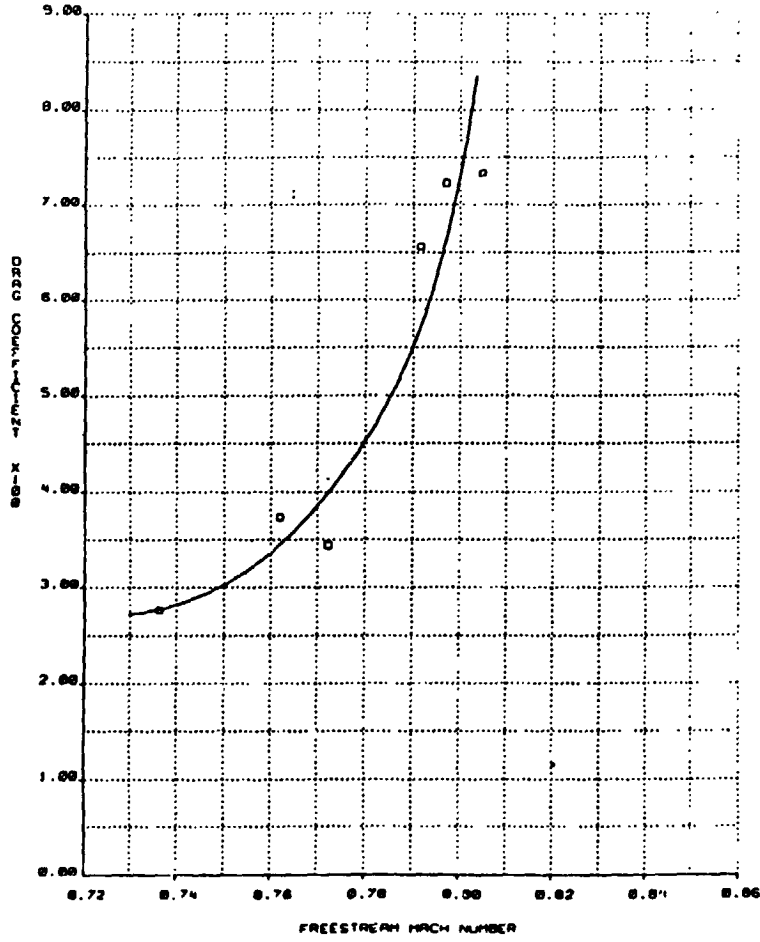
Figure 19c   Drag Coefficient vs. Freestream Mach Number,
             1.42% Linear Porosity.

Figure 19d   Drag Coefficient vs. Freestream Mach Number,
Comparison of Porosities

Figure 20   Static Pressure Ratio vs. Freestream Mach Number
for 0% and 2.8% Uniform Porosities
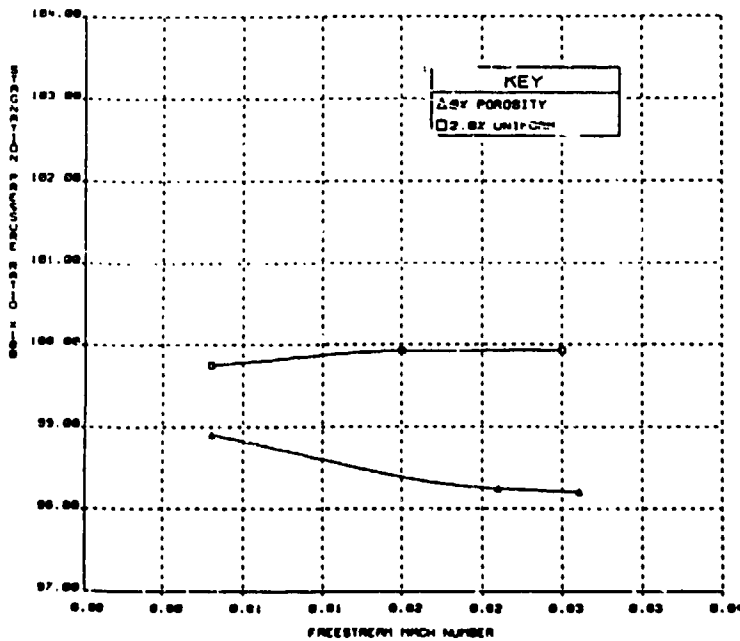
Figure 21   Total Stagnation Pressure Ratio vs. Freestream Mach
Number for 0% and 2.8% Uniform Porosities

Figure 22   Mach Number Distribution over Airfoil Corrected
for Total Pressure Losses Across Shock, $M_\infty = 0.826$
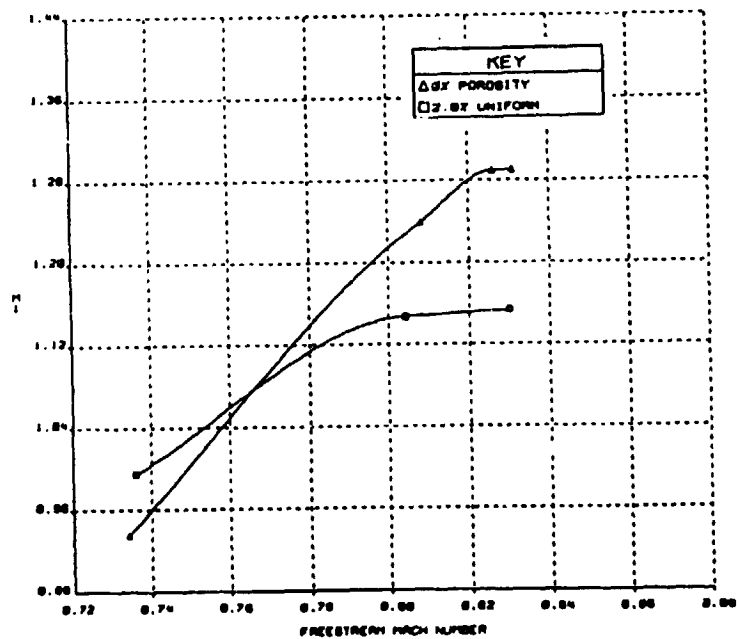
Figure 23   Critical Mach Number Determination for 0% and 2.8%
Uniform Porosities

Figure 24   Local Tunnel Mach Number vs. Distance from Inlet
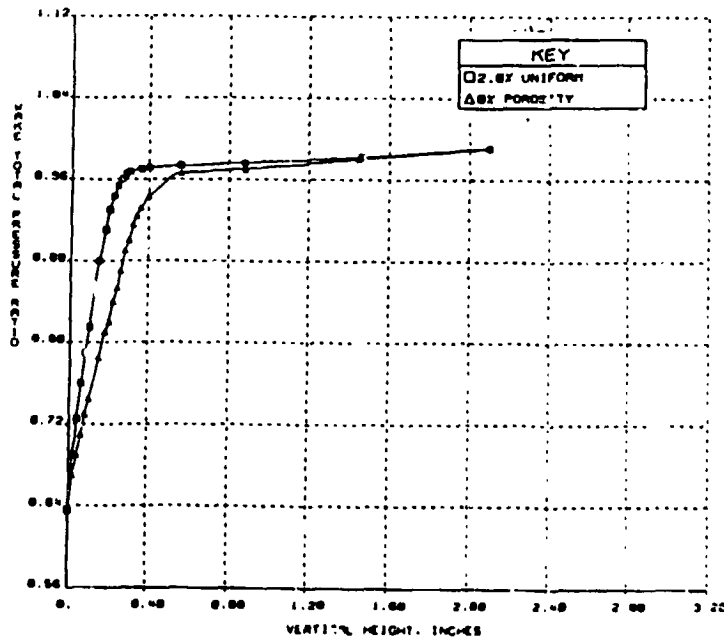
Figure 25   Wake Total Pressure Ratio Distributions for 0% and
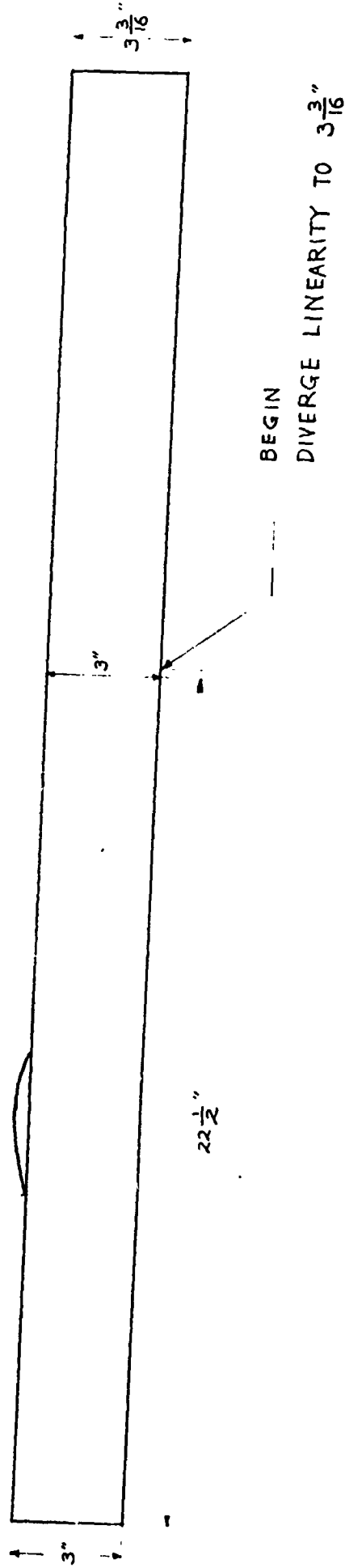2.8% Uniform Porosities, $M_\infty = 0.804$

MATERIAL : MAHOGANY

Figure 26 Transonic Tunnel Insert
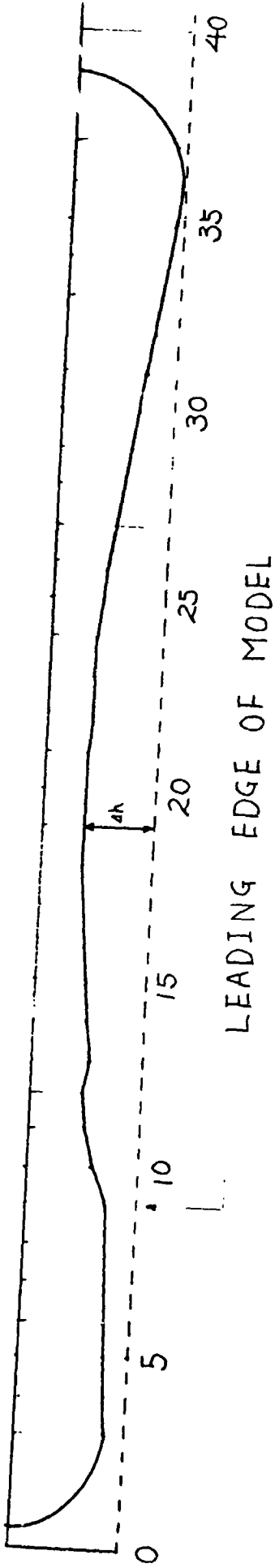
LEADING EDGE OF MODEL

ORIGINAL PAGE IS
OF POOR QUALITY

BEGIN
DIVERGE LINEARITY TO $3\frac{3}{16}$"

SCALE 1:4 (IN INCHES)
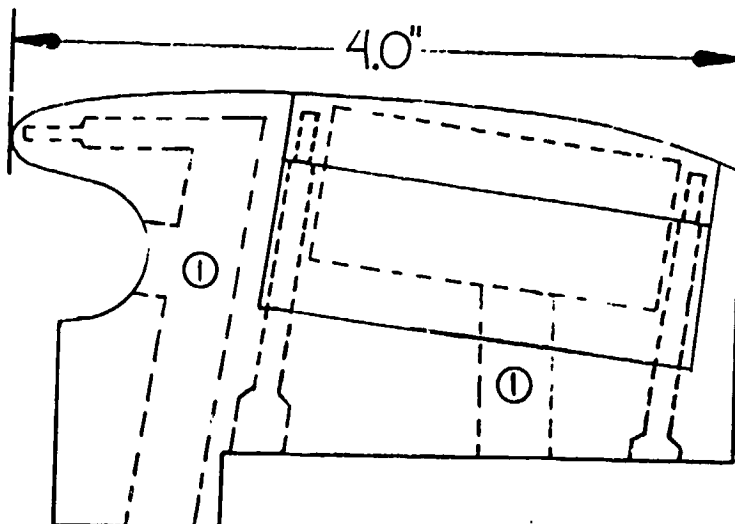
$3\frac{3}{16}$"

3"

$22\frac{1}{2}$"

3"

ADJUSTMENT SCREW TURNS VS MACH NUMBER
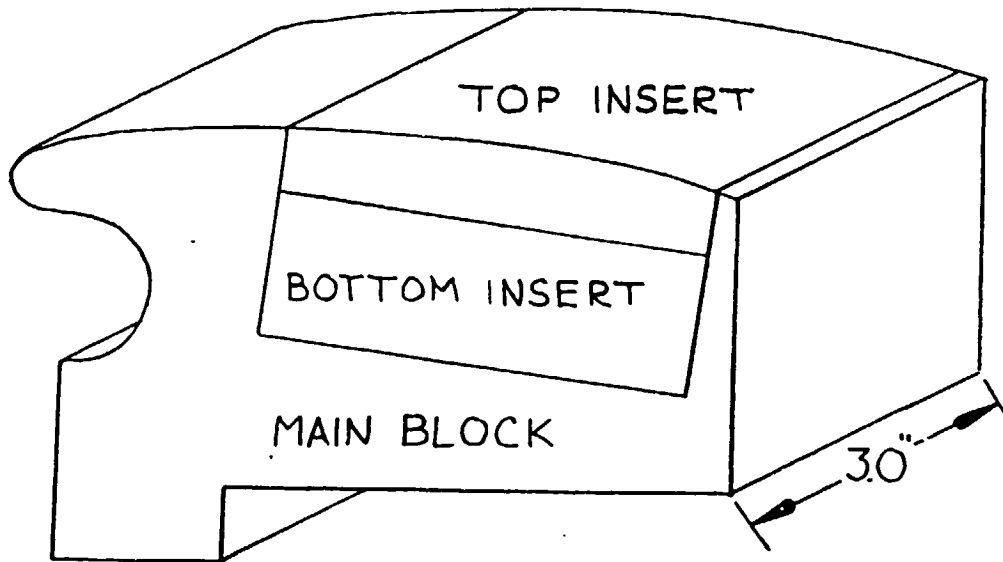

Figure 27   Adjustment screw Turns vs. Mach Number

Figure 28   Supercritical Airfoil with Removable Insert

① TAP ACCESS HOLE

Figure 29   Assembly

① TOP INSERT
② SLEEVE
③ BOTTOM INSERT
④ MAIN BLOCK
⑤ SCREWS